

# The effects of $r$ -process heating on fall-back accretion in compact object mergers

B. D. Metzger<sup>1\*</sup>, A. Arcones<sup>2,3</sup>, E. Quataert<sup>1</sup>, G. Martínez-Pinedo<sup>3</sup>

<sup>1</sup>*Astronomy Department and Theoretical Astrophysics Center, University of California, Berkeley, 601 Campbell Hall, Berkeley CA, 94720*

<sup>2</sup>*Institut für Kernphysik, TU Darmstadt, Schlossgartenstr. 9, D-64289 Darmstadt, Germany*

<sup>3</sup>*GSI Helmholtzzentrum für Schwerionenforschung, Planckstr. 1, D-64291 Darmstadt, Germany*

Accepted . Received ; in original form

## ABSTRACT

We explore the effects of  $r$ -process nucleosynthesis on fall-back accretion in neutron star(NS)-NS and black hole-NS mergers, and the resulting implications for short-duration gamma-ray bursts (GRBs). Though dynamically important, the energy released during the  $r$ -process is not yet taken into account in merger simulations. We use a nuclear reaction network to calculate the heating (due to  $\beta$ -decays and nuclear fission) experienced by material on the marginally-bound orbits nominally responsible for late-time fall-back. Since matter with longer orbital periods  $t_{\text{orb}}$  experiences lower densities, for longer periods of time, the total  $r$ -process heating rises rapidly with  $t_{\text{orb}}$ , such that material with  $t_{\text{orb}} \gtrsim 1$  seconds can become completely unbound. Thus,  $r$ -process heating fundamentally changes the canonical prediction of an uninterrupted power-law decline in the fall-back rate  $\dot{M}_{\text{fb}}$  at late times. When the timescale for  $r$ -process to complete is  $\gtrsim 1$  second, the heating produces a complete cut-off in fall-back accretion after  $\sim 1$  second; if robust, this would imply that fall-back accretion cannot explain the late-time X-ray flaring observed following some short GRBs. However, for a narrow, but physically plausible, range of parameters, fall-back accretion can *resume* after  $\sim 10$  seconds, despite having been strongly suppressed for  $\sim 1 - 10$  seconds after the merger. This suggests the intriguing possibility that the gap observed between the prompt and extended emission in short GRBs is a manifestation of  $r$ -process heating.

**Key words:** nuclear reactions, nucleosynthesis, abundances–gamma rays: bursts

## 1 INTRODUCTION

One of the most important discoveries made with the *Swift* satellite is that short- and long-duration gamma-ray bursts (GRBs) originate from distinct stellar progenitors. While long duration GRBs track ongoing star formation (e.g. Fructer et al. 2006) and result from the deaths of massive stars (e.g. Woosley & Bloom 2006), short-duration GRBs have now been localized to both early (Bloom et al. 2006; Berger et al. 2005) and late-type (Fox et al. 2005; Barthelmy et al. 2005) host galaxies, indicating a more evolved progenitor population (e.g. Prochaska et al. 2006).

Although the origin of short GRBs remains unknown, the most popular and well-studied central engine model is the binary merger of two neutron stars (NS-NS; Eichler et al. 1989; Meszaros & Rees 1992; Narayan et al. 1992) or a NS and a black hole (NS-BH; Paczyński 1991; Mochkovitch

et al. 1993). This model is qualitatively consistent with both the host galaxy properties of short GRBs (Nakar et al. 2006) and the notable lack of a bright associated supernova in some well-studied cases (e.g. Hjorth et al. 2005). Depending on the detailed properties of the binary and the (unknown) supra-nuclear density equation of state, NS-NS/NS-BH mergers result in a central compact object (either a BH or hyper-massive NS) surrounded by a compact  $\sim 10^{-3} - 0.1M_{\odot}$  disk (e.g. Ruffert et al. 1996; Rosswog et al. 1999; Lee & Kluźniak 1999; Rosswog 2005; Faber et al. 2006; Shibata & Taniguchi 2006; see Lee & Ramirez-Ruiz 2007 and Faber et al. 2009 for recent reviews). The similarity between the estimated accretion timescale of this remnant torus and the typical duration of short GRBs ( $T_{90} \sim 0.1 - 1$  seconds) has also been used as evidence in favor of compact object merger models (Narayan et al. 1992).

This clean picture has grown complex with the discovery that short GRBs are often followed by a “tail” of emission (usually soft X-rays) starting  $\sim 10$  seconds after the

\* E-mail: bmetzger@astro.berkeley.edu

GRB and lasting for  $\sim 30 - 100$  seconds (Norris & Bonnell 2006; Gehrels et al. 2006). While only  $\sim 1/4$  of *Swift* short bursts show evidence for this extended emission, the observational limits are consistent with most bursts possessing an X-ray tail with a fluence comparable to that of the prompt GRB (Perley et al. 2009). Due to its rapid variability and other similarities to the prompt gamma-ray emission, the extended emission probably results from ongoing central engine activity. However, such a significant energy output on long timescales is difficult to explain in NS-NS/NS-BH merger models, most notably because the accretion disk is blown apart by a powerful outflow after only a few seconds of viscous evolution (Metzger, Piro, & Quataert 2008, 2009; Beloborodov 2008; Lee et al. 2009).

One idea proposed for producing late-time activity is the “fall-back” of material ejected during the merger into highly eccentric (but gravitationally-bound) orbits (Rosswog 2007; Lee & Ramirez-Ruiz 2007). If the ejected mass  $M$  has a distribution of energies  $dM/d|E| \propto |E|^{-\alpha}$ , matter with  $E < 0$  produces a late-time accretion rate  $\dot{M}$  onto the central object that decreases as a power-law in time:  $\dot{M} \propto (dM/dE)(d|E|/dt_{\text{orb}}) \propto t^{-[(5+2\alpha)/3]}$  (Rees 1988), where  $t_{\text{orb}}$  is the bound ejecta’s orbital period or fall-back time. Indeed, a number of NS-NS/NS-BH merger calculations find that the fall-back at late-times may be sufficient to explain the extended emission from short GRBs via continued accretion (Faber et al. 2006; Rosswog 2007; Lee et al. 2009; see, however, Rossi & Begelman 2009).

Fall-back accretion models rely on the assumption that matter ejected onto orbits with fall-back times  $t_{\text{orb}} \gg 1$  second remains bound. However, the gravitational binding energy of such long-period orbits is only

$$|E| = \frac{GMm_n}{2a} \simeq 1.0 \left( \frac{M}{3M_\odot} \right)^{2/3} \left( \frac{t_{\text{orb}}}{1\text{ s}} \right)^{-2/3} \frac{\text{MeV}}{\text{nucleon}}, \quad (1)$$

where  $t_{\text{orb}} = 2\pi(a^3/GM)^{1/2}$ ,  $a$  is the semi-major axis of the orbit, and  $M$  and  $m_n$  are the central object mass and nucleon mass, respectively.

The *unbound* ejecta from NS-NS/NS-BH mergers has long been considered a promising source for producing very heavy elements via rapid neutron capture (*r*-process) nucleosynthesis (Lattimer & Schramm 1974, 1976; Eichler et al. 1989; Freiburghaus et al. 1999). The total nuclear energy available via the *r*-process ( $\sim 1 - 3$  MeV nucleon $^{-1}$ ; see eq. [2]) greatly exceeds  $|E|$  for orbits with  $t_{\text{orb}} \gtrsim 0.3 - 1$  second. As a result, *r*-process heating could have a crucial impact on the properties of late-time fall-back, an effect that has not yet been taken into account.

In this paper, we examine the effects of *r*-process nucleosynthesis on fall-back accretion in NS-NS/NS-BH mergers. In §2 we describe the nucleosynthesis that occurs during the decompression from nuclear densities, and the extent to which NS-NS/NS-BH merger simulations properly capture the resulting energy release. This motivates §3, in which we present calculations of *r*-process heating along orbits that are nominally responsible for late-time fall-back. In §4 we discuss our results and their implications.

## 2 DECOMPRESSION & R-PROCESS HEATING

Most of the material ejected when a NS is tidally disrupted originates from the NS’s neutron-rich outer core, which has a typical electron fraction  $Y_e \sim 0.1$  set by  $\beta$ -equilibrium

under highly degenerate conditions (Pethick & Ravenhall 1995; Haensel & Zdunik 1990a,b). Since the temperature remains fairly low as the ejecta expands (due to adiabatic losses),  $Y_e$  probably remains low ( $\sim 0.03 - 0.20$ ) during the decompression from nuclear densities (Ruffert et al. 1997; Rosswog 2005).

Schematically, the nucleosynthesis of decompressing neutron-rich matter can be divided into two stages:

(1) *Initial Decompression and Seed Formation* (density  $\rho \gtrsim \rho_{\text{drip}} \sim 4 \times 10^{11}$  g cm $^{-3}$ ). During the earliest phases of decompression, very neutron-rich nuclei form, which rapidly emit neutrons as the material expands to lower density (Lattimer et al. 1977; Meyer 1989). Heavy “seed” nuclei are then formed through ( $n, \gamma$ ) reactions and, possibly, through charged-particle reactions in full nuclear statistical equilibrium (NSE). For example, Meyer (1989) finds seed nuclei with average charges and masses  $\bar{Z} \sim 40 - 70$  and  $\bar{A} \sim 90 - 110$  (depending primarily on  $Y_e$  and the expansion rate; cf. Goriely et al. 2004), while Freiburghaus et al. (1999) finds seeds with  $Z \approx 31 - 37$  and  $A \approx 92 - 112$ . Since the seed nuclei and neutron mass fractions are given by  $X_s = \bar{A}Y_e/\bar{Z}$  and  $X_n = 1 - X_s$ , respectively, the neutron mass fraction after initial decompression is large:  $X_n \sim 0.3 - 0.9$  for plausible ranges in the values of  $\bar{A}$ ,  $\bar{Z}$ , and the electron fraction ( $Y_e \sim 0.03 - 0.2$ ; Ruffert et al. 1997; Rosswog 2005).

(2) *Rapid Neutron Capture (r-process)* ( $\rho \lesssim \rho_{\text{drip}}$ ). Once the density decreases below neutron-drip,  $\beta$ -decay channels begin opening in full, and a conventional *r*-process begins (see, e.g., Cowan, Thielemann, & Truran 1991 and Meyer 1994 for reviews). In the *r*-process, very heavy nuclei (with peaks at  $A \sim 130$  and 200) are formed when the seed nuclei rapidly capture the free neutrons remaining from stage 1. This establishes an ( $n, \gamma$ ) equilibrium, with  $\beta$ -decays driving the nucleosynthetic “flow” to larger  $Z$  on longer timescales, with possible “fission cycling” between nuclei with  $A \sim 280$  and  $A \sim 130 - 140$ .

If NSE is assumed, the nuclear energy released when seeds form (stage 1) can be captured in numerical simulations of NS-NS/NS-BH mergers by employing an appropriate equation of state (EOS). For instance, the NS-NS merger simulations of Rosswog et al. (1999) use a Lattimer-Swesty (1991) EOS, which accounts for the possible presence of protons, neutrons,  $\alpha$ -particles, and a single average “heavy” nucleus. As a result, they find that the ejected tidal tails “explode” due to the energy released as seed nuclei form. Since the Shen EOS (Shen et al. 1998a,b) employed by Rosswog & Davies (2002; cf. Rosswog 2005) captures similar physics, the effects of seed nuclei formation are already taken into account in the fall-back estimates of Rosswog (2007).

However, the subsequent *r*-process has the potential to generate a comparable or greater amount of energy. In particular, once all of the synthesized nuclei decay back to stable isotopes, the total nuclear energy released and available to heat the ejecta is

$$\Delta E_r \simeq (1 - f_\nu) \left[ \left( \frac{B}{A} \right)_r - X_s \left( \frac{B}{A} \right)_s - X_n \Delta_n \right], \quad (2)$$

where  $\Delta_n = (m_n - m_p)c^2 = 1.293$  MeV is the neutron-proton mass difference, and  $\left( \frac{B}{A} \right)_{s,r}$  are appropriately-averaged binding energies for the seed and *r*-process nuclei, respectively. The factor  $f_\nu$  is the fraction of the nuclear energy lost to neutrinos and is  $\sim 0.5$  (see §3.2). Using typical val-

ues of  $\left(\frac{E}{A}\right)_r \approx 8 \text{ MeV nuc}^{-1}$  and  $\left(\frac{E}{A}\right)_s \approx 8.7 \text{ MeV nuc}^{-1}$ , we estimate that  $\Delta E_r \approx 1 - 3 \text{ MeV nuc}^{-1}$  for  $X_n$  in the range  $\sim 0.3 - 0.9$ .

Comparing  $\Delta E_r$  with the binding energy of the fall-back material (eq. [1]), we conclude that if the  $r$ -process goes to completion, it will strongly affect the *dynamics* of orbits with  $t_{\text{orb}} \gtrsim 0.3 - 1$  seconds. Unlike seed nuclei formation, the effects of  $r$ -process heating cannot be readily incorporated into merger simulations, in part because most of the energy is released on length and time scales exceeding that which can be presently simulated. More importantly, because the  $r$ -process is a non-equilibrium process involving a large number of exotic nuclei, its study requires a complex reaction network, which would be prohibitive to include in multi-dimensional simulations. In the next section we explore the  $r$ -process heating of bound ejecta by performing nucleosynthesis calculations along a few representative Lagrangian density trajectories.

### 3 NUCLEOSYNTHESIS CALCULATIONS

#### 3.1 Density Trajectories

When the less massive NS is tidally disrupted during a NS-NS or NS-BH merger, a portion of the stellar material is ejected into one or two long tidal tail through the outer Lagrange points (Lattimer & Schramm 1974). This material is imparted with a distribution of energies (or, equivalently for bound material, semi-major axes  $a$ ). Initially, all of the ejecta (bound and unbound) is approximately spatially coincident (at an assumed pericenter distance  $r_p \approx 10^7 \text{ cm}$ ) and shares a common density during decompression. Thus, during the early expansion we use the density trajectory  $\rho(t)$  corresponding to the *unbound* ejecta studied in  $r$ -process calculations by Freiburghaus et al. (1999) and taken from the NS-NS merger simulations of Rosswog et al. (1999).

On later timescales, material with energy  $E < 0$  and fall-back time  $t_{\text{orb}} \propto |E|^{-3/2}$  spatially decouples from the unbound ejecta, once their orbits approach apocenter. Motivated by simulations (e.g. Rosswog 2007) and theoretical considerations (Rees 1988), we assume  $dM/d|E| \propto \text{constant}$ , corresponding to a fall-back rate of

$$\begin{aligned} \dot{M}_{\text{fb}} &\simeq \left(\frac{dM}{dE}\right) \left(\frac{d|E|}{dt_{\text{orb}}}\right) \\ &\approx 10^{-2} M_{\odot} \text{ s}^{-1} \left(\frac{dM/dE}{10^{-2} M_{\odot}/\text{MeV nuc}^{-1}}\right) \left(\frac{t_{\text{orb}}}{1 \text{ s}}\right)^{-5/3} \quad (3) \end{aligned}$$

where we normalize  $dM/dE$  so that  $\sim 10^{-2} M_{\odot}$  returns to the central object on a timescale  $\gtrsim 1$  second (absent the effects of  $r$ -process heating), as is required in models that attribute late-time X-ray tails from short GRBs to fall-back (e.g. Rosswog 2007; Faber et al. 2006; Lee et al. 2009).

The mass-flux along a series of trajectories with a given fall-back time  $t_{\text{orb}}$  can also be written as

$$\dot{M} = \Delta\Omega \rho v r^2, \quad (4)$$

where  $r(t)$  and  $v(t)$  are the radius and velocity of the orbit, and  $\Delta\Omega(t)$  is the spread in solid angle of bound fluid elements. By equating equations (3) and (4) we obtain the *late-time* density trajectory. Our ignorance of the details of the merger (which depends on uncertainties such as the NS EOS) and the effects of nuclear energy input on the ejecta

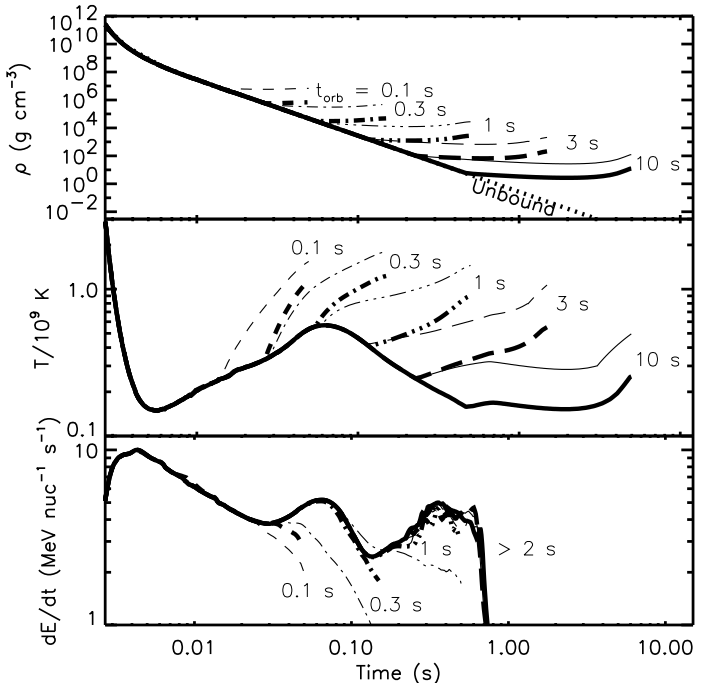


**Figure 1.**  $r$ -process nucleosynthesis in bound ejecta from compact object mergers. (*Upper Panel*) Lagrangian density trajectories  $\rho(t)$  employed in our nucleosynthesis calculations, shown for ejecta with different initial orbital periods  $t_{\text{orb}} = 0.1 \text{ s}$  (short dashed lines),  $0.3 \text{ s}$  (dash-dot lines),  $1 \text{ s}$  (triple-dot-dash lines),  $3 \text{ s}$  (long dashed lines), and  $10 \text{ s}$  (solid lines) and for two values for the orbits' solid angle  $\Delta\Omega = 4\pi, 4\pi/10$  (darker and lighter shaded lines, respectively). The trajectory of the unbound material (which all orbits share at early times) is shown with a dotted line. (*Middle Panel*) Temperature evolution for the trajectories shown in the upper panel. (*Bottom Panel*) Total  $r$ -process heating rate (due to  $\beta$ -decays and nuclear fission) for the trajectories shown in the upper panel, assuming that  $1/2$  of the energy is lost to neutrinos (see §3.2).

trajectories are parameterized with  $\Delta\Omega(t)$ . For simplicity we assume that  $\Delta\Omega$  is constant with time because our results are relatively insensitive to this choice. We choose a relatively large value for  $\Delta\Omega \sim 4\pi/10 - 4\pi$ , motivated by the large dispersion in the bound ejecta's orbital parameters expected to result from the explosive energy release during seed formation (§2) and the subsequent  $r$ -process heating. We only calculate heating until the orbits reach apocenter because we are primarily interested in the total energy release, and  $r$ -process heating decreases rapidly once material re-compresses on its return to pericenter. The top panel of Figure 1 shows the density trajectories employed in our calculations for a variety of fall-back times.

#### 3.2 Network Calculations

We use a dynamical  $r$ -process network calculation (Martinez-Pinedo 2008; Petermann et al. 2008) that includes neutron captures, photodissociations,  $\beta$ -decays, and fission reactions. The latter includes contributions from neutron induced fission,  $\beta$  delayed fission, and spontaneous fission. All heating is self-consistently added to the entropy of the fluid following the procedure of Freiburghaus et al. (1999). The change of temperature is determined using the Timmes

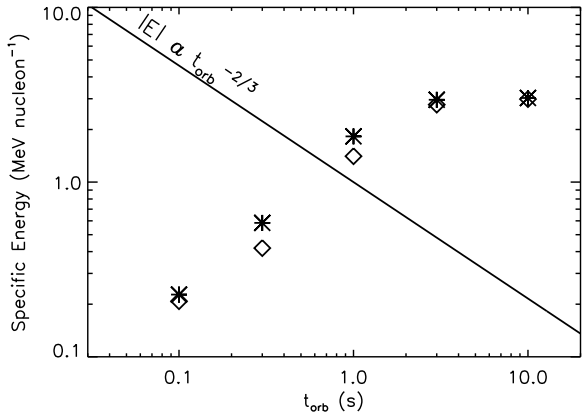


**Figure 2.** Total  $r$ -process heating  $\Delta E$  as a function of initial orbital period (or nominal fall-back time)  $t_{\text{orb}}$  for the nucleosynthesis calculations shown in Figure 1, shown for  $\Delta\Omega = 4\pi$  (asterisks) and  $4\pi/10$  (diamonds). The binding energy of the orbit  $|E|$  (eq. [1]) is shown for comparison with a solid line (for an assumed  $M = 3M_{\odot}$  central object).

equation of state (Timmes & Arnett 1999). Although our calculation does not explicitly account for the energy loss from  $\beta$ -decays into escaping neutrinos, we take this into account by artificially decreasing the heating rate by a factor 1/2. This is justified because most of the heating results from  $\beta$ -decays and the energy released is shared approximately equally between electrons (which thermalize) and neutrinos.

In addition to  $\rho(t)$ , the initial temperature  $T$ , electron fraction  $Y_e$ , and seed nuclei properties ( $\bar{A}, \bar{Z}$ ) are specified for a given calculation. We assume an initial temperature  $T = 4 \times 10^9$  K, although the subsequent  $r$ -process heating is not particularly sensitive to this choice (Meyer 1989; Freiburghaus et al. 1999). We also assume  $Y_e = 0.1$ ,  $\bar{Z} \simeq 36$ ,  $\bar{A} \simeq 118$  (see §2). Varying the electron fraction and the properties of the seed nuclei will quantitatively affect the subsequent  $r$ -process heating (e.g. through the total available energy; eq. [2]); the implications of this are discussed in §4.2.

### 3.3 Results

The middle and bottom panels of Figure 1 show the time evolution of the temperature  $T$  and heating rate  $\dot{E}$ , respectively. The temperature initially decreases rapidly due to the adiabatic expansion. However, as the expansion rate decreases, nuclear energy generation reheats the ejecta to  $T \approx 5 \times 10^8$  K. At this point a difference develops between trajectories with short orbital periods ( $t_{\text{orb}} \lesssim 1$  s) and long orbital periods ( $t_{\text{orb}} \gtrsim 1$  s). For short orbital periods the density approaches an approximately constant value relatively quickly. At constant density all of the generated energy is used to increase the temperature, which reaches a value  $T \gtrsim 10^9$  K. At these high temperatures photodissociation reactions become important and the  $r$ -process path moves closer to stability. This decreases the beta-decay rates and Q-values, and, consequently, the heating rate decreases. For the longest period orbits ( $t_{\text{orb}} \gtrsim 1$  s), there is a balance

between energy generation and adiabatic losses, which keeps the temperature almost constant.

Also note that  $\dot{E}$  remains relatively constant in the range  $\sim 2 - 5$  MeV nucleon $^{-1}$  s $^{-1}$  throughout most of the sampled trajectories for  $t \lesssim 1$  second. This illustrates that the total  $r$ -process heating  $\Delta E = \int_0^{t_{\text{orb}}/2} \dot{E} dt$  is dominated by relatively late times in the orbit, and that  $\Delta E$  is approximately proportional to  $t_{\text{orb}}$ . Note that at  $t \approx 0.7$  second  $\dot{E}$  sharply decreases once neutrons are exhausted and the  $r$ -process is effectively complete.

The total  $r$ -process heating is shown explicitly in Figure 2, which plots  $\Delta E$  for the trajectories from Figure 1 as a function of orbital period. The orbital binding energy  $|E| \propto t_{\text{orb}}^{-2/3}$  (eq. [1]) is plotted for comparison with a solid line. Note that  $\Delta E$  rises rapidly with  $t_{\text{orb}}$  for both values of  $\Delta\Omega$ , before saturating at  $\Delta E_r \approx 3$  MeV (eq. [2]) for  $t_{\text{orb}} \gtrsim 2$  seconds; material with  $t_{\text{orb}} \gtrsim 1$  second experiences sufficient heating to become unbound.

## 4 DISCUSSION AND IMPLICATIONS

### 4.1 Fall-Back Accretion

Figure 2 illustrates that orbits with initial periods exceeding a fraction of a second experience sufficient  $r$ -process heating to become unbound. However, this does not by itself guarantee a suppression in the fall-back rate  $\dot{M}_{\text{fb}}$  at late times because the marginally-bound material ejected by the  $r$ -process (with initial orbital energy  $|E_i| < \Delta E$ ) could in principle simply be replaced by material that was initially more tightly bound ( $|E_i| \gtrsim \Delta E$ ). It is also important to understand how the effects of  $r$ -process heating differ from that of seed nucleus formation; both release comparable amounts of the energy, yet seed formation is already incorporated in merger calculations and does not produce a sharp cut-off in the fall-back rate (Rosswog 2007).

Although our  $r$ -process calculations assumed ballistic ejecta (§3.1), this approximation is no longer valid once significant energy is added to the orbit (i.e., if  $\Delta E \sim |E_i|$ ). Because the ejecta is optically-thick, most of the deposited thermal energy is transferred into kinetic energy via adiabatic expansion. This puts the ejecta on less-bound orbits which, due to their lower densities and longer periods, experience even more  $r$ -process heating (Fig. 1). This suggests that the  $r$ -process may lead to a run-away in which all material with an initial orbital period exceeding a threshold value will acquire sufficient energy to become unbound.

To explore these issues quantitatively, we consider a toy model to calculate  $\dot{M}_{\text{fb}}$  including the effects of  $r$ -process heating. We consider an ensemble of mass elements  $dM$  distributed with initial energies  $E_i$  according to  $dM/d|E_i| \propto \text{constant}$  (as in eq. [3]). The final energy of each mass element at apocenter is given by

$$E_f = E_i + \int_0^{t_{\text{orb}}(E)/2} \dot{E} dt, \quad (5)$$

where  $\dot{E}(t)$  is the heating rate along the orbit. As discussed in §3.3 and shown in Figures 1 and 2,  $\dot{E}$  is roughly constant in time along an orbit (for  $t \lesssim 1$  s). Thus, we make the simplifying assumption that  $\dot{E} = \Delta E_r / t_{\text{heat}}$  for  $t \leq t_{\text{heat}}$  and  $\dot{E} = 0$  for  $t > t_{\text{heat}}$ , where  $\Delta E_r$  is the total available

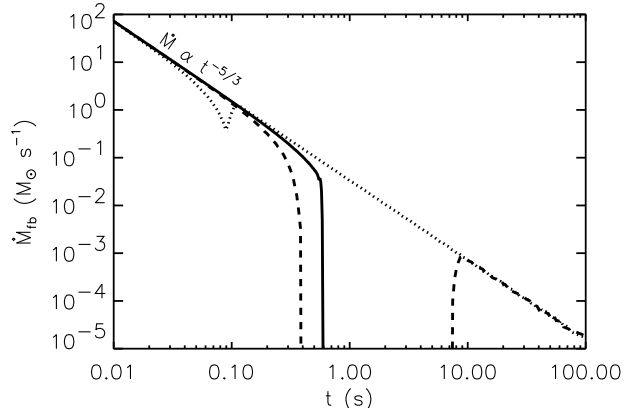


**Figure 3.** Fall-back rate  $\dot{M}_{\text{fb}}$  in NS-NS/NS-BH mergers including the effects of  $r$ -process heating, as calculated using the toy model described in §4.1. Each model assumes a  $M = 3M_{\odot}$  central object and that the total available  $r$ -process energy is  $\Delta E_r = 3$  MeV. Different line styles correspond to different heating timescales:  $t_{\text{heat}} = 0.1$  seconds (*dotted line*), 0.86 seconds (*dashed line*), and 3 seconds (*solid line*).

$r$ -process energy (eq. [2]) and  $t_{\text{heat}}$  is the timescale for  $r$ -process heating (which we leave as a free parameter). Our results presented below are relatively insensitive to the precise functional form of  $\dot{E}$  prior to  $t_{\text{heat}}$  provided that the total heating is dominated by late times in the orbit.

If the final energy at apocenter  $E_f$  is  $< 0$  for a given mass element, it remains bound despite  $r$ -process heating, with a new fall-back time which we approximate as  $t_{\text{orb}}(E_f)$ . If, on the other hand,  $E_f > 0$  the particle is unbound from the central object and does not contribute to late-time accretion. Note that because the upper limit of integration in equation (5) increases with the orbital energy, this model allows for the run-away effect described above.

Figure 3 shows our results for  $\dot{M}_{\text{fb}}$  with  $r$ -process heating, calculated for fixed  $\Delta E_r = 3$  MeV and for several values of  $t_{\text{heat}}$ . Because tightly-bound material with short orbital periods experiences little  $r$ -process heating,  $\dot{M}_{\text{fb}}$  at early times is unaffected by the  $r$ -process and decreases at the canonical rate  $\propto t^{-5/3}$  for all values of  $t_{\text{heat}}$ . At late-times, however, there is a bifurcation in the behavior of  $\dot{M}_{\text{fb}}$ : short heating times ( $t_{\text{heat}} \ll 0.9$  s) lead to a relatively uninterrupted power law decline, while long heating times ( $t_{\text{heat}} > 0.9$  s) produce a sharp cut-off in the fall-back rate.

The origin of this bifurcation can be understood by noting the existence of a critical orbit distinguishing material that necessarily experiences the full heating available  $\Delta E_r$  from those that may not. When  $r$ -process heating is active, the energy of an orbit evolves as  $E = -|E_i| + \dot{E}t$ . As time increases, the magnitude of the orbital energy decreases, i.e.,  $|E|$  goes down, and thus the orbital period increases. There is a critical orbit for which the  $r$ -process heating leads to the orbital period increasing so rapidly with time that the orbit can never actually reach apocenter ( $t = t_{\text{orb}}/2$ ) as long as  $r$ -process heating is active. These orbits necessarily receive the full  $r$ -process heating  $\Delta E_r$ . This critical orbital energy  $E_c$  can be determined by setting  $dt/d|E| = 1/2(dt_{\text{orb}}/d|E|)$  using equation (1) and  $E = -|E_i| + \dot{E}t$ . This implies

$$|E_c| \simeq 1.35 \text{ MeV} \left( \frac{M}{3M_{\odot}} \right)^{2/5} \left( \frac{\Delta E_r}{3 \text{ MeV}} \right)^{2/5} \left( \frac{t_{\text{heat}}}{1 \text{ s}} \right)^{-2/5}. \quad (6)$$

The *initial* orbital energy for which  $E_c$  is just reached at apocenter is given by  $E(t = t_{\text{orb}}/2) = E_i + \dot{E}t_{\text{orb}}/2 = E_c$ , which implies  $|E_{i,c}| = 5|E_c|/3$ . Note that equation (6) can be estimated on dimensional grounds by solving for  $E_i$  such that  $|E_i| \approx (\Delta E_r/t_{\text{heat}})t_{\text{orb}}(E_i)/2$ .

There is a bifurcation in the behavior for  $|E_i| < |E_{i,c}|$  and  $|E_i| > |E_{i,c}|$ . Orbits with  $|E_i| < |E_{i,c}|$  necessarily receive the full heating and so have  $E_f = -|E_i| + \Delta E_r$ , while those with  $|E_i| > |E_{i,c}|$  may or may not (see below). The orbital period (or fall-back time) corresponding to  $|E_c|$  is given by

$$t_{\text{orb},c} \simeq 0.6 \text{ s} \left( \frac{M}{3M_{\odot}} \right)^{2/5} \left( \frac{\Delta E_r}{3 \text{ MeV}} \right)^{-3/5} \left( \frac{t_{\text{heat}}}{1 \text{ s}} \right)^{3/5}, \quad (7)$$

from which it follows that

$$\frac{t_{\text{heat}}}{t_{\text{orb},c}} \simeq 1.7 \left( \frac{M}{3M_{\odot}} \right)^{-2/5} \left( \frac{\Delta E_r}{3 \text{ MeV}} \right)^{3/5} \left( \frac{t_{\text{heat}}}{1 \text{ s}} \right)^{2/5}. \quad (8)$$

If  $t_{\text{heat}} \ll t_{\text{orb},c}$  then any material with  $t_{\text{orb}} > t_{\text{orb},c}$  has already experienced the full heating  $\Delta E_r$  earlier in its orbit. In this case, there is a slight decrease in  $\dot{M}_{\text{fb}}$  around the time at which  $t_{\text{orb}} \sim t_{\text{heat}}$ , but there is no significant interruption in the fall-back rate; this corresponds to  $t_{\text{heat}} = 0.1$  s in Figure 3. In particular,  $\dot{M}_{\text{fb}}$  still decreases as a power-law  $\propto t^{-5/3}$  at late times because adding a constant energy to each  $dM$  simply renormalizes the energy scale when  $dM/dE$  is flat. This explains why seed nucleus formation, which occurs on roughly the initial expansion timescale  $\sim$  milliseconds  $\ll t_{\text{orb},c}$ , has little effect on the rate that  $\dot{M}_{\text{fb}}$  decreases at late times.

On the other hand, if  $t_{\text{heat}} \gg t_{\text{orb},c}$  then an absolute cut-off in  $dM/d|E_f|$  (and hence  $\dot{M}_{\text{fb}}$ ) occurs for  $E_f \gtrsim E_c$ , corresponding to times  $t \gtrsim t_{\text{orb},c}$ . This case is well-illustrated by the  $t_{\text{heat}} = 3$  s model in Figure 3.

In intermediate cases, when  $t_{\text{heat}} \sim t_{\text{orb},c}$  (i.e.,  $|E_{i,c}| \sim \Delta E_r$ ), there is still cut-off in the accretion, but material with  $|E_i| \gtrsim |E_{i,c}|$  may remain marginally-bound despite the extra energy it receives, thus leading to a temporal gap in  $\dot{M}_{\text{fb}}(t)$ . This is illustrated by the  $t_{\text{heat}} = 0.86$  s model in Figure 3, which shows a long delay between the cut-off in accretion at  $t \approx 0.4$  s and its resumption at  $t \approx 10$  s. We find, however, that the gap only exists for a fairly narrow range of parameters, and, when present, its width  $\Delta t_{\text{gap}}$  is exponentially sensitive to  $t_{\text{heat}}/t_{\text{orb},c}$ ; e.g., increasing  $t_{\text{heat}}/t_{\text{orb},c}$  from 1.3 to 1.7 increases  $\Delta t_{\text{gap}}$  from  $\sim 1$  to  $\sim 100$  s.

From our calculations in §3 we find that  $\Delta E_r \approx 3$  MeV and  $t_{\text{heat}} \approx 0.7$  s, which corresponds to  $t_{\text{heat}} \sim 1.5t_{\text{orb},c}$ . This is at the boundary between the “absolute cut-off” and “intermediate” regimes described above and shown in Figure 3. We discuss the implications of this result in the next section.

## 4.2 Implications for the Origin of Short GRBs with Extended Emission

Our primary conclusion is that fall-back accretion following NS-NS/NS-BH mergers is suppressed on timescales exceeding  $\sim 0.3 - 1$  seconds due to  $r$ -process heating. This result has important implications for the origin of extended X-ray emission observed  $\sim 10 - 100$  seconds following some short GRBs. As discussed in the Introduction, standard merger

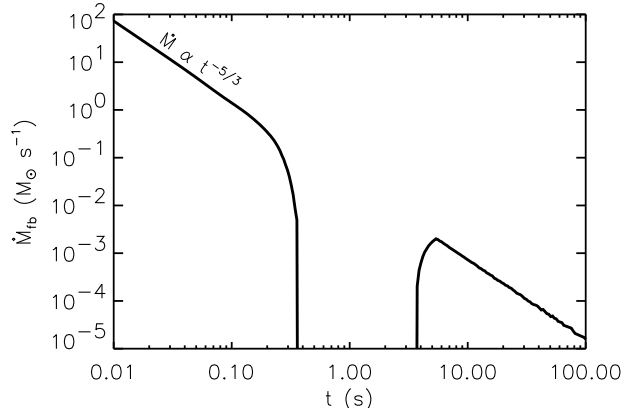


**Figure 4.** Fall-back rate  $\dot{M}_{\text{fb}}$  calculated using the model from §4.1 taking  $\dot{E}(t)$  directly from our  $r$ -process calculations in Figure 1 for the  $t_{\text{orb}} = 10$  s orbit.

models have difficulty explaining activity on such a late timescale, which has led to the suggestion that late-time flaring is powered by fall-back (Faber et al. 2006; Rosswog 2007; Lee et al. 2009). If long heating timescales and/or high values of  $\Delta E_r$  obtain (such that  $t_{\text{heat}} > 2t_{\text{orb,c}}$ ), our results strongly disfavor this explanation because the cut-off in  $\dot{M}_{\text{fb}}$  is absolute: very little material returns to the central object at late times (see the solid line in Fig. 3).

This conclusion changes, however, if  $\Delta E_r$  is lower and/or  $t_{\text{heat}}$  is shorter, such that  $t_{\text{heat}} \lesssim 2t_{\text{orb,c}}$ . In this case, the  $r$ -process produces a temporal gap in the fallback rate instead of an absolute cut-off (Fig. 3). Intriguingly, the extended emission following short GRBs shows a lull of  $\sim 3$ – $10$  seconds between the end of the GRB and the beginning of the extended emission (e.g. Norris & Bonnell 2006; Gehrels et al. 2006; Perley et al. 2009). Attributing this delay to  $r$ -process heating appears, however, to require fine-tuned parameters:  $t_{\text{heat}}/t_{\text{orb,c}}$  must be between  $\sim 1.5$ – $1.7$  in order for the temporal gap to have a duration of 3–30 seconds. Nevertheless, typical parameters for  $r$ -process heating are not far from the critical condition  $t_{\text{heat}} \sim t_{\text{orb,c}}$ .

To illustrate this explicitly, Figure 4 shows  $\dot{M}_{\text{fb}}(t)$  calculated using the simple model described in §4.1, but using  $\dot{E}$  directly from our  $r$ -process calculations in Figure 1 for  $t_{\text{orb}} = 10$  seconds. For these particular parameters, the exact  $\dot{E}(t)$  suppresses fall-back accretion from  $\sim 0.4$ – $4$  seconds, but fall-back then resumes at late times. Although the properties of the gap are quite sensitive to the parameters of the  $r$ -process heating, the presence of a gap may in fact be rather robust, because the parameters on which  $t_{\text{heat}}$  and  $t_{\text{orb,c}}$  depend ( $\Delta E_r, M, t_{\text{heat}}$ ) may not vary substantially from event to event. For instance, the outer portions of a NS ejected during a NS-NS/NS-BH merger are probably highly neutron-rich and likely remain so during the expansion (Ruffert et al. 1997). For low  $Y_e$  the total energy released by the  $r$ -process asymptotes to the value  $\Delta E_r \approx 0.5[(B/A)_r - \Delta_n] \approx 3.3$  MeV (provided that  $Y_e$  is not sufficiently low that the  $r$ -process freezes-out before all neutrons are captured). Furthermore, for a merger to produce a significant accretion disk (as is required to produce a GRB), the mass of the central black hole or NS proba-

bly must lie in the relatively narrow range  $M \sim 3$ – $10M_{\odot}$  (e.g. Rantsiou et al. 2009). Finally, a heating timescale of  $\approx 1$  second also appears to be robust, relatively independent of uncertainties such as  $\Delta\Omega$  (see Fig. 2);  $t_{\text{heat}} \approx 1$  second was also found in an independent  $r$ -process calculation employing somewhat different assumptions and physics (see Goriely et al. 2004; their Fig. 3). Further work is thus clearly required to assess the possibility that the gap between the prompt and extended emission in short GRBs is a manifestation of  $r$ -process heating. In particular, given the sensitivity of the late-time fall-back rate to the  $r$ -process heating, it is important to consider a range of initial  $Y_e$  and seed nuclei in the  $r$ -process calculations, and to improve on the simple model in §4.1 by carrying out hydrodynamic calculations of fall-back using simplified models of the  $r$ -process heating rate.

If future work indicates that  $r$ -process heating produces a robust sharp cut-off in  $\dot{M}_{\text{fb}}$  (with no late-time resumption), our results may instead suggest that the central engine in some short GRBs is a long-lived NS rather than a BH, because the former could remain active even in the absence of surrounding matter. For instance, the massive central object that forms in a NS-NS merger could be temporarily supported by differential rotation (e.g., Baumgarte et al. 2000; Duez et al. 2004, 2006) or remain stable indefinitely if it loses sufficient mass via a centrifugally-driven outflow (e.g. Thompson et al. 2004; Dessart et al. 2008). Another possibility for producing a stable NS is via the accretion-induced collapse (AIC) of a white dwarf. In either AIC or NS-NS mergers, if the rapidly-rotating NS is strongly magnetized, its electromagnetic spin-down could plausibly power the observed extended emission (Usov 1992; Metzger, Quataert, & Thompson 2008). If AIC occurs following a double white dwarf merger, late-time emission could also be powered by the accretion of material left over after the merger, which has an accretion timescale  $\sim 100$  seconds (Metzger, Quataert, & Thompson 2008).

## ACKNOWLEDGMENTS

We thank R. Hix, J. Lattimer, W. Lee, and T. Rauscher for helpful discussions and information. BDM and EQ were partially supported by the Packard Foundation. AA and GMP were partially supported by the Deutsche Forschungsgemeinschaft through contract SFB 634 and by the Helmholtz Alliance of the Extreme Matter Institute (EMMI).

## REFERENCES

- Barthelmy, S. D., et al. 2005, *Nature*, 438, 994
- Baumgarte, T. W., Shapiro, S. L., & Shibata, M. 2000, *ApJL*, 528, L29
- Beloborodov, A. M. 2008, *AIP Conference Series*, 1054, 51
- Berger, E., et al. 2005, *Nature*, 438, 988
- Bloom, J. S., et al. 2006, *ApJ*, 638, 354
- Bloom, J. S., & Prochaska, J. X. 2006, *Gamma-Ray Bursts in the Swift Era*, 836, 473
- Cowan, J. J., Thielemann, F.-K., & Truran, J. W. 1991, *Physics Reports*, 208, 267
- Dessart, L., Burrows, A., Ott, C. D., Livne, E., Yoon, S.-C., & Langer, N. 2006, *ApJ*, 644, 1063
- Dessart, L., Burrows, A., Livne, E., & Ott, C. D. 2008, *ApJL*, 673, L43

- Duez, M. D., Liu, Y. T., Shapiro, S. L., Shibata, M., & Stephens, B. C. 2006, *Phys. Rev. D*, 73, 104015
- Duez, M. D., Liu, Y. T., Shapiro, S. L., & Stephens, B. C. 2004, *Phys. Rev. D*, 69, 104030
- Eichler, D., Livio, M., Piran, T., & Schramm, D. N. 1989, *Nature*, 340, 126
- Faber, J. 2009, *Classical and Quantum Gravity*, 26, 114004
- Faber, J. A., et al. 2006, *ApJL*, 641, L93
- Fruchter, A. S., et al. 2006, *Nature*, 441, 463
- Fox, D. B., et al. 2005, *Nature*, 437, 845
- Freiburghaus, C., Rosswog, S., & Thielemann, F.-K. 1999, *ApJL*, 525, L121
- Gehrels, N., et al. 2006, *Nature*, 444, 1044
- Goriely, S., Demetriou, P., Janka, H.-T., Pearson, J. M., & Samyn, M. 2005, *Nuclear Physics A*, 758, 587
- Haensel, P., & Zdunik, J. L. 1990a, *A&A*, 227, 431
- Haensel, P., & Zdunik, J. L. 1990b, *A&A*, 229, 117
- Hjorth, J., et al. 2005, *ApJL*, 630, L117
- Lattimer, J. M., Mackie, F., Ravenhall, D. G., & Schramm, D. N. 1977, *ApJ*, 213, 225
- Lattimer, J. M., & Schramm, D. N. 1974, *ApJL*, 192, L145
- Lattimer, J. M., & Schramm, D. N. 1976, *ApJ*, 210, 549
- Lattimer, J. M., & Douglas Swesty, F. 1991, *Nuclear Physics A*, 535, 331
- Lee, W. H., & Kluźniak, W. 1999, *ApJ*, 526, 178
- Lee, W. H., Ramirez-Ruiz, E., & López-Cámara, D. 2009, *ApJL*, 699, L93
- Lee, W. & Ramirez-Ruiz, E. 2007, *New J. Phys.*, 9, 17
- Martínez-Pinedo, G. 2008, *Eur. Phys. J. Special Topics* 156, 123
- Meszáros, P., & Rees, M. J. 1992, *ApJ*, 397, 570
- Metzger, B. D., Piro, A. L., & Quataert, E. 2008, *MNRAS*, 390, 781
- Metzger, B. D., Piro, A. L., & Quataert, E. 2009, *MNRAS*, 396, 304
- Metzger, B. D., Quataert, E., & Thompson, T. A. 2008, *MNRAS*, 385, 1455
- Meyer, B. S. 1989, *ApJ*, 343, 254
- Meyer, B. S. 1994, *ARAA*, 32, 153
- Mochkovitch, R., Hernanz, M., Isern, J., & Martin, X. 1993, *Nature*, 361, 236
- Nakar, E., Gal-Yam, A., & Fox, D. B. 2006, *ApJ*, 650, 281
- Nakar, E. 2007, *PhR*, 442, 166
- Narayan, R., Paczyński, B., & Piran, T. 1992, *ApJL*, 395, L83
- Norris, J. P., & Bonnell, J. T. 2006, *ApJ*, 643, 266
- Paczyński, B. 1991, *Acta Astronomica*, 41, 257
- Perley, D. A., et al. 2009, *ApJ*, 696, 1871
- Petermann, I., et al. 2008, *arXiv:0812.0968*
- Pethick, C. J., & Ravenhall, D. G. 1995, *Annu. Rev. Nucl. Part. Sci.*, 45, 429
- Prochaska, J. X., et al. 2006, *ApJ*, 642, 989
- Rantsiou, E., Kobayashi, S., Laguna, P., & Rasio, F. A. 2008, *ApJ*, 680, 1326
- Rees, M. J. 1988, *Nature*, 333, 523
- Rossi, E. M., & Begelman, M. C. 2009, *MNRAS*, 392, 1451
- Rosswog, S. 2005, *ApJ*, 634, 1202
- Rosswog, S. 2007, *MNRAS*, 376, L48
- Rosswog, S., Liebendörfer, M., Thielemann, F.-K., Davies, M. B., Benz, W., & Piran, T. 1999, *A&A*, 341, 499
- Rosswog, S., Ramirez-Ruiz, E., & Davies, M. B. 2003, *MNRAS*, 345, 1077
- Rosswog, S., & Davies, M. B. 2002, *MNRAS*, 334, 481
- Rosswog, S., Speith, R., & Wynn, G. A., 2004, *MNRAS*, 351, 1121
- Ruffert, M., Janka, H.-Th., & Schäfer, G. 1996, *A&A*, 311, 532
- Ruffert, M., Janka, H.-T., Takahashi, K., & Schaefer, G. 1997, *A&A*, 319, 122
- Sato, K. 1974, *Progress of Theoretical Physics*, 51, 726
- Shen, H., Toki, H., Oyamatsu, K., & Sumiyoshi, K. 1998, *Progress of Theoretical Physics*, 100, 1013
- Shen, H., Toki, H., Oyamatsu, K., & Sumiyoshi, K. 1998, *Nuclear Physics A*, 637, 435
- Shibata, M. & Taniguchi, K. 2006, *Phys. Rev. D*, 73, 064027
- F. X. Timmes & D. Arnett, *ApJS* 125, 277 (1999)
- Thompson, T. A., Chang, P., & Quataert, E. 2004, *ApJ*, 611, 380
- Usov, V. V. 1992, *Nature*, 357, 472
- Woosley, S. E., & Bloom, J. S. 2006, *Annual Rev. of A&A*, 44, 507